Estimating Aerodynamic Characteristics of the ALFLEX Vehicle using Flight Test Data

Masaaki YANAGIHARA*1, Masashi SHIGEMI*1,
Hidehiko NAKAYASU*2

ABSTRACT

One of the purposes of the Automatic Landing Flight Experiment (ALFLEX) was to estimate aerodynamic characteristics of a vehicle with a delta wing and tip fins. The tests for this purpose, such as α / β sweep tests and control surface exciting tests were conducted during the hanging flights and automatic landing flights. By analyzing the flight test data obtained at Woomera test area in Australia, the aerodynamic characteristics of the ALFLEX vehicle are estimated and the results are compared with those predicted from the wind tunnel tests. As a result, the estimated characteristics are similar to the predicted ones except for a few characteristics. Although the results extracted from the hanging flights were scattered due to the measurement errors caused by the effects of an umbilical cable, the method will be useful if the problem is solved by a means such as using an inner battery.

1. Introduction

The purposes of the Automatic Landing Flight Experiment (ALFLEX[1]) were: 1) evaluation of low-speed aerodynamic characteristics of a vehicle with a delta wing and tip fins, 2) establishment and demonstration of the unmanned automatic landing technology, and 3) evaluation of flight experiment methodology using a scaled model. For those purposes, three phases of flight tests, preliminary hanging flight tests in Japan, hanging flight tests in Australia and automatic landing flight tests in Australia were conducted from October 1995 to August 1996. In this paper, the aerodynamic characteristics of the ALFLEX vehicle estimated using the flight test data obtained at Woomera test area in Australia are presented and they are compared with the wind-tunnel database which was used for designing the vehicle and its flight control system.

2. Hanging Flight Test

2.1 Flight Test for Aerodynamic Characteristics Estimation Performed in Hanging Flight

A Hanging flight is a flight test in which the vehicle is suspended by a hanging wire through gimbals with 2 axes set at the designed C.G. (Center of Gravity) point and flies with a freedom of rotation around the pitch, roll and yaw axes. In the hanging flights dynamic flight tests and quasi-steady flight tests are performed to estimate the aerodynamic characteristics.

Dynamic flight tests are conducted to identify an aerodynamic model including dynamic effects, and control surface exciting tests where an M-sequence signal (pseudo random rectangular signal) was inputted to elevator, aileron or rudder and α, β or Φ command step input tests were performed. All of these tests are to excite a dynamic maneuver and an aerodynamic model which has a certain analytic model structure will be fit to the recorded data using a least-squares method and model parameters are estimated[2]. Figure 2.1-1 shows the data of flight C006 as an example of the elevator exciting test. Although the elevator behaves as if a pulse signal is inputted because the flight control system of the vehicle, which is always engaged during the flight, outputs an inverse command signal to stabilize the motion due to the input signal when the rectangular signal is inputted,

*1 National Aerospace Laboratory
*2 National Space Development Agency of Japan

the vehicle performs a pitching maneuver in response to elevator input. As the dynamic flight tests, two trials of elevator exciting test, three trials of α command step input test, one trial each of aileron and rudder exciting test, three trials of β command step input test and two trials of Φ command step input test were conducted.

Quasi-steady flight tests are needed to investigate the trimmed flight characteristics of the vehicle, and α sweep tests to estimate the longitudinal characteristics and β sweep tests to estimate the lateral-directional characteristics are carried out. In the sweep tests, the attitude of the vehicle is altered quasi-statically by changing the α or β command to the control system gradually. As the rate is kept small, the vehicle maintains a trimmed flight condition while changing the attitude. The recorded angles of the control surfaces and the aerodynamic coefficients calculated using the recorded accelerations show the trimmed flight characteristics. Figure 2.1-2 shows time histories of the α sweep test conducted during flight C004. As the quasi-steady tests, three trials each of α and β sweep tests were carried out.

2.2 Aerodynamic Characteristics Estimated from Hanging Flight

Tables 2.2-1 and 2.2-2 show the aerodynamic model structures used for aerodynamic model identification using the dynamic flight data obtained in the hanging flights and parameter values of an analytical aerodynamic model obtained by fitting these model structures to the flight test data (hereinafter referred to as the "HF identified

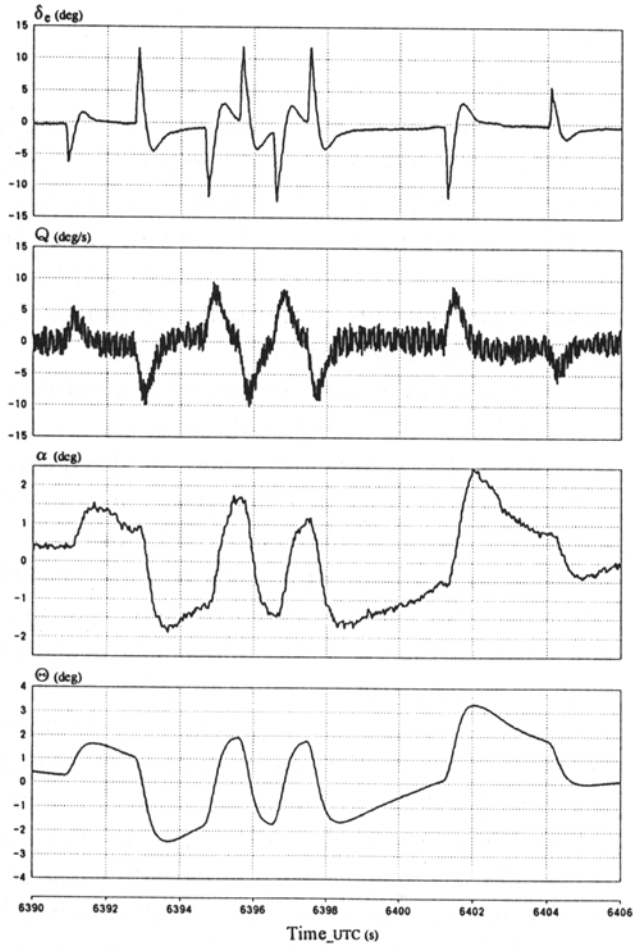

Fig. 2.1-1 Elevator M-Sequence Input Test (Hanging Flight)

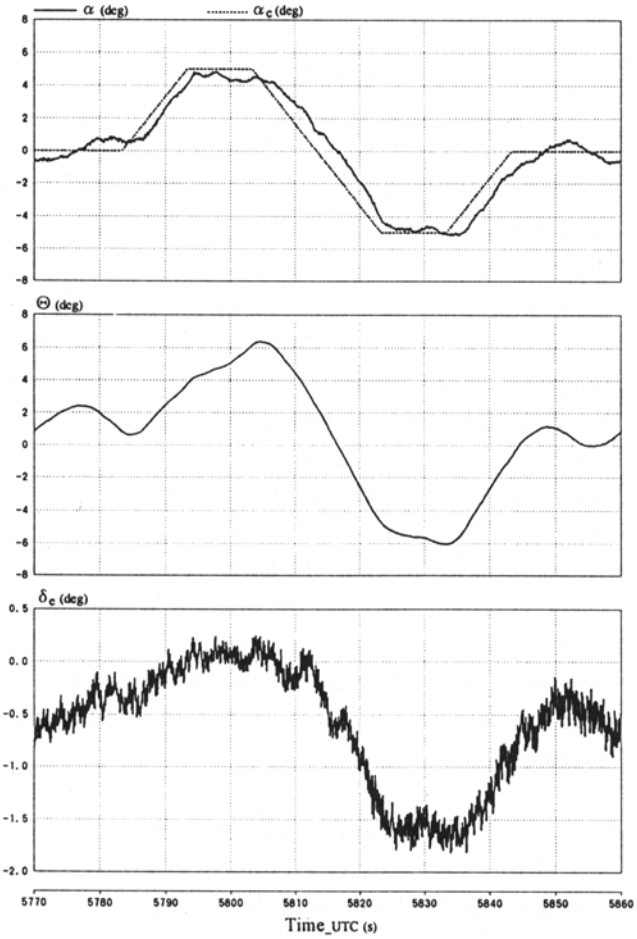

Fig. 2.1-2 α Sweep Test (Hanging Flight)

model"). The tables also show the parameter values of a analytical aerodynamic model (hereinafter referred to as the "predicted model") obtained by fitting the same model structures to a functional aerodynamic model gained based on the wind-tunnel test (hereinafter referred to as the "wind-tunnel model"). For obtaining the longitudinal predicted model, the model structures are fitted to the wind-tunnel model in the range of angle of attack from -6 to +14 degrees which is the range used in the dynamic flight tests in the hanging flights. As the lateral-directional characteristics change very much with the angle of attack, the lateral-directional predicted model is calculated using the wind-tunnel model at $\alpha = 0^\circ$ because the control system was used to maintain the angle of attack at 0° during the flight tests for the estimation of the lateral-directional characteristics. The values inside parentheses in the row of the predicted parameters are the uncertainties of the wind-tunnel database. They are estimated errors between the wind-tunnel data and the real characteristics of the vehicle (tolerance). Values inside parentheses in the row of the estimated parameters indicate three times the standard deviation (3σ) of the least-squares estimator of the parameters. For dynamic parameters of the lateral-directional models, only Cl_p and Cn_r are estimated fixing the cross terms, Cl_r and Cn_p at the values of the predicted model because it is difficult to separate roll and yaw motions. Figures 2.2-1 and 2.2-2 show the major parameters in Tables 2.2-1 and 2.2-2 graphically. In these figures a white circle with a black border and bars in both sides of the circle denote the predicted parameter and the uncertainties of the wind-tunnel database (tolerance), and a cross indicates the estimated parameter. The absence of tolerance bars indicates that the uncertainties are not defined. Figures 2.2-3 and 2.2-4 show the relation between

Table 2.2-1 Longitudinal Aerodynamic Model (Hanging Flight)

Longitudinal Aerodynamic Model Structure

$$C_L = C_{L_0} + C_{L_\alpha}\cdot\alpha + C_{L_{\delta e}}\cdot\delta e + C_{L_{\delta s}}\cdot\delta s$$
$$C_D = C_{D_0} + C_{D_{\alpha 2}}\cdot\alpha^2 + C_{D_\alpha}\cdot\alpha + C_{D_{\delta e}}\cdot\delta e + C_{D_{\delta s}}\cdot\delta s$$
$$C_m = C_{m_0} + C_{m_{\alpha 2}}\cdot\alpha^2 + C_{m_\alpha}\cdot\alpha + C_{m_q}\cdot\hat{q} + C_{m_{\delta e}}\cdot\delta e + C_{m_{\delta s}}\cdot\delta s$$

Longitudinal Aerodynamic Model Parameters

	C_{L_0}	$C_{L_{\alpha 2}}$	C_{L_α}	C_{L_q}	$C_{L_{\delta e}}$	$C_{L_{\delta s}}$
Prediction (Tolerance)	−0.086 (0.022)	–	2.093 (0.401)	–	0.697 (0.180)	−0.057
Estimation (3σ)	−0.082 (0.001)	–	2.028 (0.008)	–	0.515 (0.018)	–

	C_{D_0}	$C_{D_{\alpha 2}}$	C_{D_α}	C_{D_q}	$C_{D_{\delta e}}$	$C_{D_{\delta s}}$
Prediction (Tolerance)	0.068 (0.007)	0.997	−0.083	–	0.036	0.060
Estimation (3σ)	0.056 (0.000)	1.318 (0.031)	−0.164 (0.006)	–	−0.031 (0.007)	–

	C_{m_0}	$C_{m_{\alpha 2}}$	C_{m_α}	C_{m_q}	$C_{m_{\delta e}}$	$C_{m_{\delta s}}$
Prediction (Tolerance)	−0.002 (0.010)	−0.181	0.089 (0.121)	−0.761	−0.233 (0.060)	0.017
Estimation (3σ)	−0.001 (0.000)	−0.099 (0.006)	0.038 (0.001)	−0.895 (0.032)	−0.189 (0.001)	–

Table 2.2-2 Lateral-Directional Aerodynamic Model (Hanging Flight)

Lateral-Directional Aerodynamic Model Structure

$$C_Y = C_{Y_0} + C_{Y_\beta}\cdot\beta + C_{Y_{\delta a}}\cdot\delta a + C_{Y_{\delta r}}\cdot\delta r$$
$$C_l = C_{l_0} + C_{l_\beta}\cdot\beta + C_{l_p}\cdot\hat{p} + C_{l_r}\cdot\hat{r} + C_{l_{\delta a}}\cdot\delta a + C_{l_{\delta r}}\cdot\delta r$$
$$C_n = C_{n_0} + C_{n_\beta}\cdot\beta + C_{n_p}\cdot\hat{p} + C_{n_r}\cdot\hat{r} + C_{n_{\delta a}}\cdot\delta a + C_{n_{\delta r}}\cdot\delta r$$

Lateral-Directional Aerodynamic Model Parameters ($\alpha = 0^\circ$)

	C_{Y_0}	C_{Y_β}	C_{Y_p}	C_{Y_r}	$C_{Y_{\delta a}}$	$C_{Y_{\delta r}}$
Prediction (Tolerance)	0.001 (0.006)	−0.661 (0.111)	–	–	−0.052 (0.010)	0.205 (0.063)
Estimation (3σ)	0.013 (0.000)	−0.795 (0.007)	–	–	−0.184 (0.018)	0.155 (0.013)

	C_{l_0}	C_{l_β}	C_{l_p}	C_{l_r}	$C_{l_{\delta a}}$	$C_{l_{\delta r}}$
Prediction (Tolerance)	−0.000 (0.004)	−0.055 (0.034)	−0.248	−0.030	−0.144 (0.022)	0.073 (0.017)
Estimation (3σ)	0.001 (0.000)	−0.039 (0.000)	−0.186 (0.011)	−0.030	−0.123 (0.001)	0.061 (0.001)

	C_{n_0}	C_{n_β}	C_{n_p}	C_{n_r}	$C_{n_{\delta a}}$	$C_{n_{\delta r}}$
Prediction (Tolerance)	−0.001 (0.001)	−0.019 (0.023)	0.163	−0.455	0.024 (0.014)	−0.110 (0.024)
Estimation (3σ)	−0.001 (0.000)	0.002 (0.001)	0.163	−0.335 (0.027)	0.025 (0.002)	−0.095 (0.001)

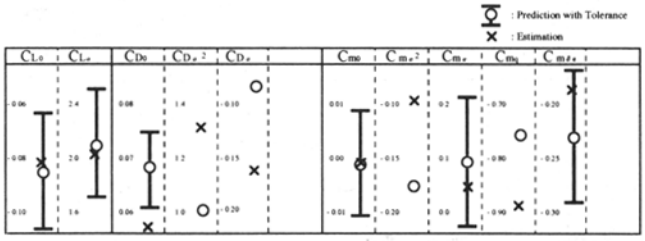

Fig. 2.2-1 Longitudinal Model Parameters (Hanging Flight)

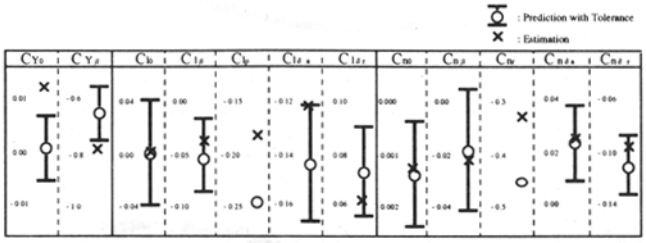

Fig. 2.2-2 Lateral-Directional Model Parameters (Hanging Flight)

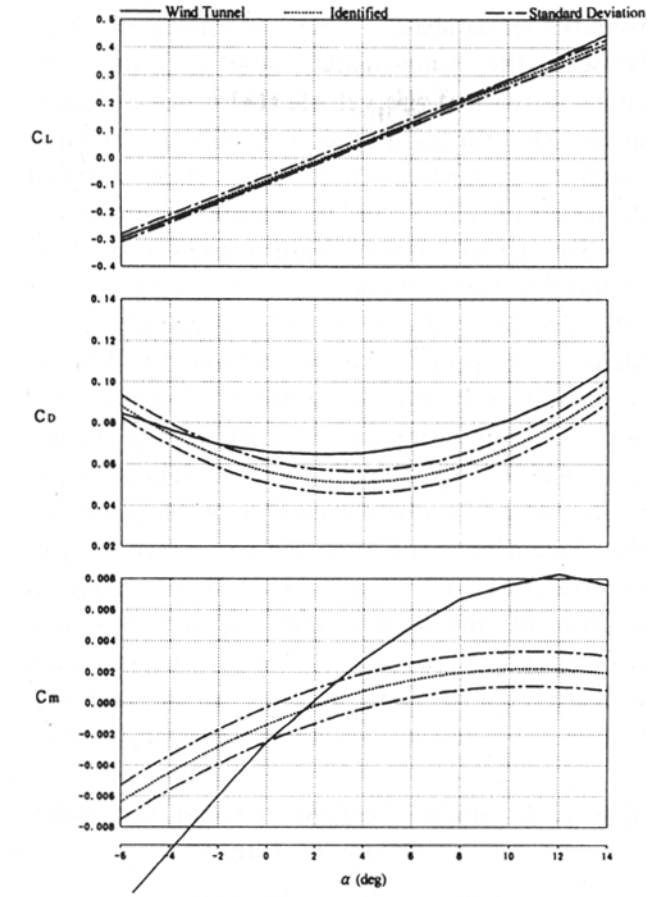

Fig. 2.2-3 Longitudinal Identified Model (Hanging Flight)

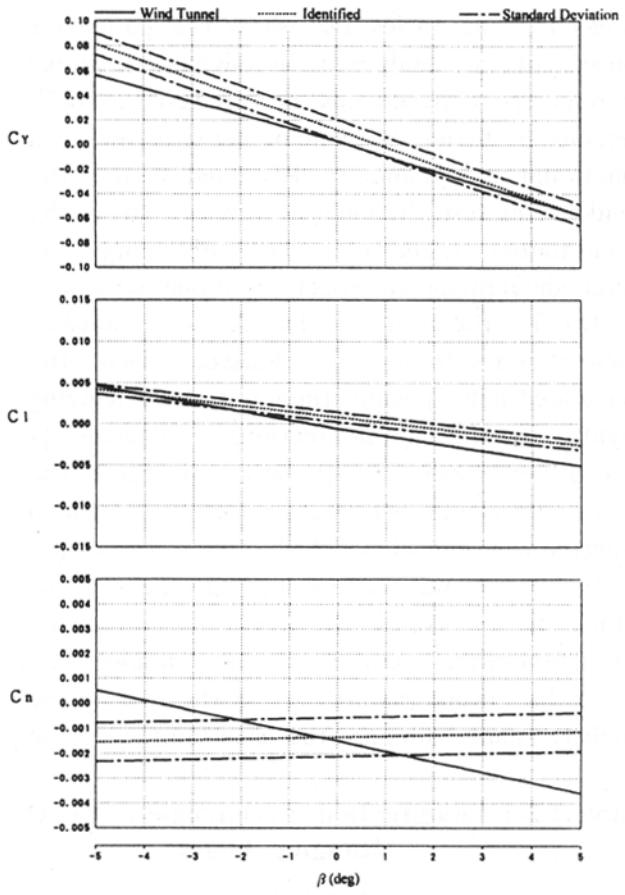

Fig. 2.2-4 Lateral-Directional Identified Model (Hanging Flight)

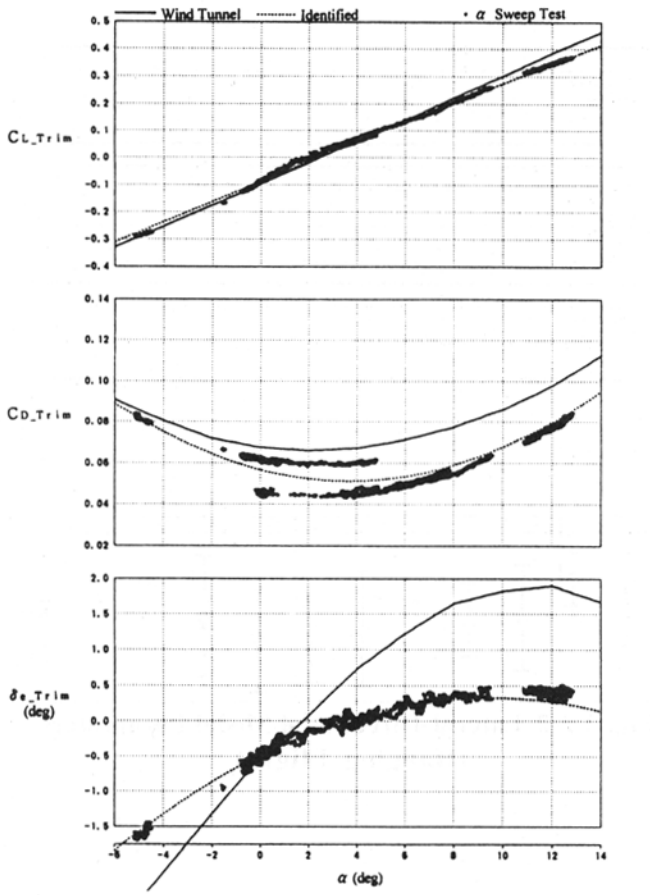

Fig. 2.2-5 Estiamted Longitudinal Trim Characteristics (Hanging Flight)

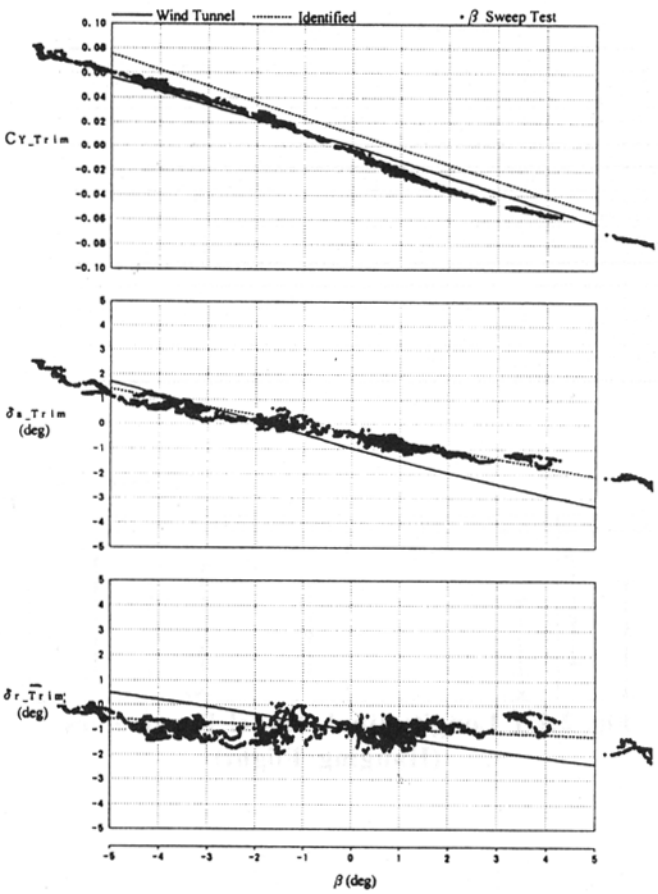

Fig. 2.2-6 Estiamted Lateral-Directional Trim Characteristics (Hanging Flight)

the HF identified model and the wind-tunnel model using α or β as an abscissa parameter. In these figures, broken lines indicate the HF identified model, solid lines indicate the wind-tunnel model and dash-dot lines indicate the standard deviation (σ) of the input data around the identified model. Figures 2.2-5 and 2.2-6 show the trimmed characteristics obtained by analyzing the α / β sweep test data. In these figures, the aerodynamic coefficients and angles of control surfaces at the trimmed flight condition calculated from the α / β sweep tests are indicated with dots using α or β as an abscissa parameter, and the trimmed characteristics calculated using the wind-tunnel model or HF identified model are also shown for reference with solid lines or broken lines, respectively. The following are the results of a study of these figures and tables.

(1) Longitudinal Characteristics

Judging from Table 2.2-1 or Fig. 2.2-1, although a difference between the estimated and predicted values for the effect of the elevator ($CL_{\delta e}$) is a little out of the tolerance, the difference for the other parameters of the lift coefficient and the pitching moment coefficient are within the tolerance and it can be said that close agreement between both models was obtained. Although the HF identified model shows a larger pitch damping (Cm_q), it is less than 120% of the predicted value and the difference is not so large. There is a large difference, however, between the estimated and predicted values of the constant term of the drag coefficient (CD_0).

In Fig. 2.2-3, the HF identified model and the predicted model show good agreement for the lift coefficient. For the drag coefficient, there are differences not only for the constant term which was seen in Table 2.2-1 or Fig. 2.2-1 but for α^2 and α terms. For the pitching moment coefficient, there seems to be a fairly large difference although all the estimated parameters are inside the predicted tolerances. It is, however, one of the reasons for this that the ordinate of the graph of the pitching moment coefficient is magnified more than usual, because the vehicle has an almost neutral pitch stability.

In the graph of trimmed characteristics (Fig. 2.2-5), the trimmed lift coefficient ($CL_{\_Trim}$) extracted from the HF identified model coincides with those extracted from the α sweep tests and the wind-tunnel model. For the trimmed elevator angle ($\delta e_{\_Trim}$), the result of the α sweep tests coincides with the result calculated using the HF identified model, and the result by the wind-tunnel model differs from the others. It can be seen that the results for the trimmed drag coefficient ($CD_{\_Trim}$) extracted from the α sweep tests separate into two groups with a bias of about 0.02. Three trials of α sweep tests were performed and the result of two of them, C004 (α =-5° ⇆ +5°) and C006 (α =0° → 12°), are indicated in this graph. The difference between these two groups for the lift characteristics and the pitching moment characteristics is not so large. As the reason for this difference seems to be some measurement error, the sensitivity analysis was carried out to identify the error source which affects the estimation of the drag characteristics but does not have so large an effect on the lift and pitching moment characteristics. As the aerodynamic force acting on the vehicle in the hanging flights is estimated by subtracting the tension of the hanging wire from the total external force (equal to the aerodynamic force in the automatic landing flight) calculated using the angular acceleration data, the load-cell and the gimbal angles necessary to calculate the tension are also the objective of the sensitivity analysis. Locations of the load-cell and the gimbals and the definition of the gimbal angles are shown in Figs. 2.2-7 and 2.2-8. The sensitivity analysis clearly showed that a bias error of the gimbal pitch angle has the largest effect on the estimation error of the drag coefficient. To confirm this, the trimmed gimbal pitch angle in all the hanging flights was investigated, and the average value of the angle at each flight varies between about 3.5 and 5.0 degrees, although the value oscillates due to the pendulum-like motion. A bias error of 1.5 degrees on the gimbal pitch angle results in an error of 0.02 for the drag estimation, consistent with Fig. 2.2-5, but results in an error of only 0.0002 for the lift estimation and has virtually no effect on the pitching moment characteristics

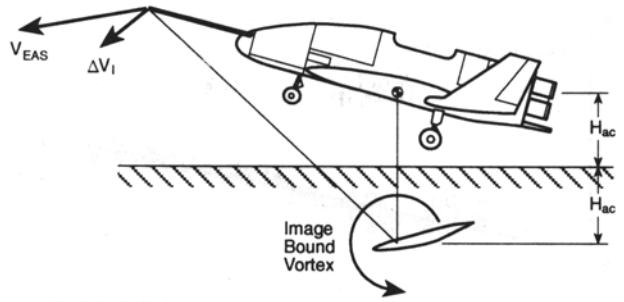

Fig. 3-2 Image-Bound Vortex Influence on the Noseboom Airspeed Sensor

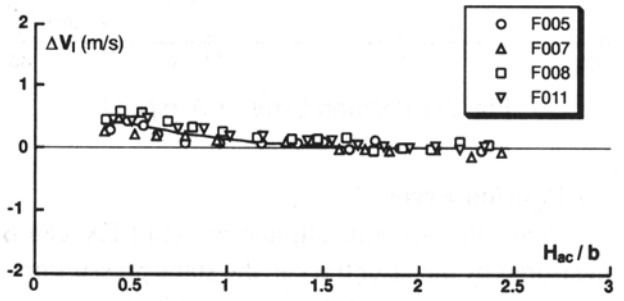

Fig. 3-3 Image-Bound Vortex Effect for Airspeed

interference between flow around the airframe and ground as the aircraft approaches the ground.

There is a radio altimeter which measures the absolute altitude with good accuracy. The radio altimeter, which played an important role in the automatic landing approach, is installed in ALFLEX. However, we cannot use the absolute altitude measured by the radio altimeter, since the bias value fluctuated.

Except for the radio altimeter, the laser tracker was installed as a ground facility which measured the position of the ALFLEX. The ALFLEX position data obtained from the laser tracker is converted into runway coordinate system which uses the end of the runway as the origin. The height above the ground can be calculated from the data of the laser tracker since the slope of the runway is known. The runway slope in the runway coordinate system was measured by using kinematic GPS on the runway center. The height above the ground of ALFLEX can be obtained by subtracting the runway slope from the height calculated from the laser tracker data in the runway coordinate system, because runway slope by measure of the kinematic GPS was given in the 5 ~ 6m interval.

3.3 Image of Bound Vortex

As the aircraft descends to touchdown, airspeed error results from the image of the bound vortex, as illustrated in Fig. 3-2. This airspeed error can be measured from the difference (ΔH_I) between the barometric altitude AGL and absolute altitude. The equation to correct airspeed using the measured pressure altitude error is given by :

$$\Delta V_I = \frac{\Delta H_I}{\frac{V_\infty^*}{g}\frac{\rho_0}{\rho}\left[1+\frac{\gamma-1}{2}\left(\frac{V_\infty^*}{a_0}\right)^2\right]^{\frac{1}{\gamma-1}}} \qquad (3.3)$$

Figure 3-3 shows this airspeed error induced by the image of the bound vortex.

4. Ground Effect Characteristics

The ground effect data must be analyzed in terms of aircraft mean aerodynamic center height (H_{ac}), because the ground effect is the aerodynamic phenomena as the aircraft nears the ground.

Figure 4-1 shows a representative example of the result of ground effect analysis for lift coefficient. The measured lift coefficient (C_L), lift coefficient in free air (C_{L_∞}) and the change in lift coefficient caused by ground effects ($\Delta C_{L_{GE}}$) in the landing approach are presented in Fig. 4-1. The horizontal axis in this figure is the normalized height defined by mean aerodynamic center height above the ground divided by the wing span (b = 3.295m).

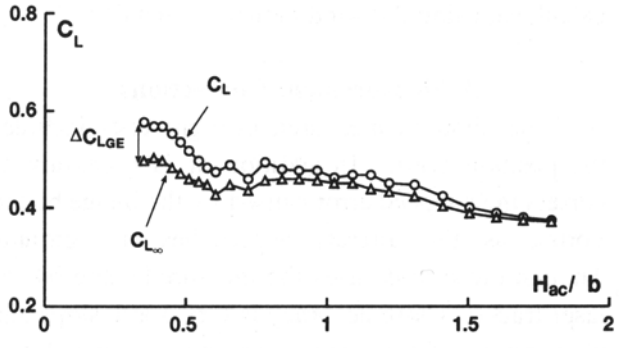

Fig. 4-1 Lift Coefficient during a Landing Approach

estimated values of the roll damping (Cl_p) and the yaw damping (Cn_r) are about 75% of the predicted values, fairly close to the predicted values.

In Fig. 2.2-4, the bias of the side force coefficient (CY) and the difference of the yawing moment slope (Cn_β) between the HF identified model and the wind-tunnel model are remarkable. The bias of the side force coefficient was also seen in the evaluation with the parameter value, and it can be seen from this figure that the scattering of the input data (dash-dot lines) are large and that the estimation is affected by it. For Cn_β, the ordinate of the graph is magnified similarly to the pitching moment in Fig. 2.2-3, and it is one of the reasons why the difference seems very large.

In Fig. 2.2-6, the trimmed aileron angle (δa_{Trim}) and the trimmed rudder angle (δr_{Trim}) calculated using the HF identified model and the results of the β sweep test agree well and these results also appear reliable, taking into account the fact that the identified model parameters are within the predicted tolerances. For the trimmed side force coefficient (CY_{Trim}), although the slope against the side slip angle of the result by the HF identified model coincide with the results of the β sweep test, there is a large bias and the result of the β sweep test agrees with the result by the wind-tunnel model rather than the identified model from this view point. This might occur because the gimbal roll angle varies from the dynamic flight test to the β sweep test as the gimbal pitch angle in the estimation of the drag coefficient. As the wind-tunnel model has smaller unsymmetricalness and agree with the results of the β sweep test, the wind-tunnel model is thought to be more reliable than the identified model.

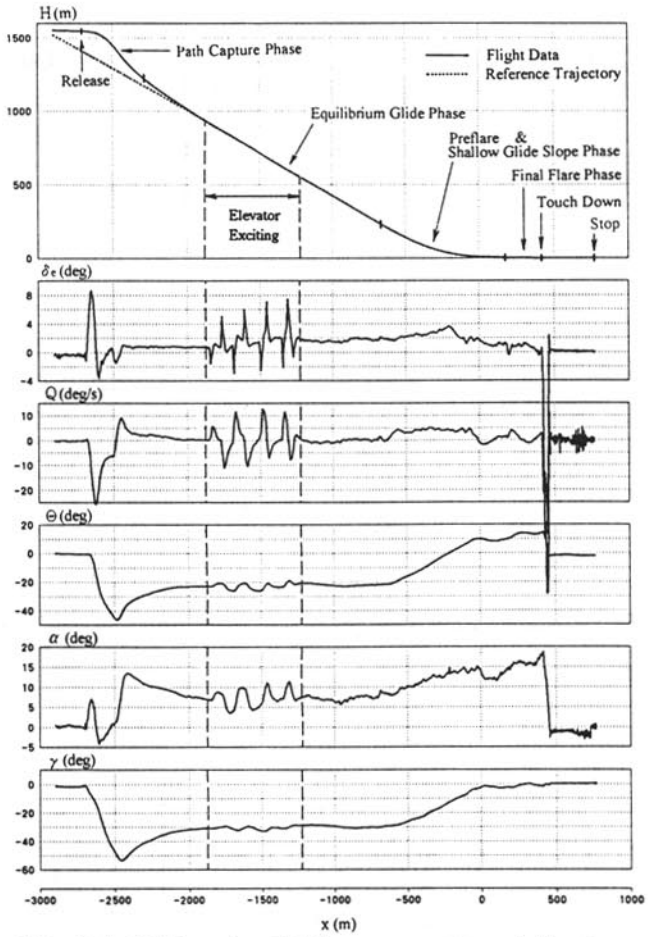

Fig. 3.1-1 Elevator M-Sequence Input Test (Automatic Landing Flight)

3. Automatic Landing Flight Test

3.1 Flight Test for Aerodynamic Characteristics Estimation Performed in Automatic Landing Flight

During the equilibrium glide phase for 15−20 seconds, the vehicle flies at a trimmed condition and there is enough time until the final landing phase when precise control is required. Utilizing some 10 seconds during this phase, the control surface exciting tests were performed. Figure 3.1-1 shows the data of flight F012 as an example of the elevator exciting test. The vehicle performs a pitching maneuver in response to elevator input, but the flight path is affected by the maneuver only slightly. Eight out of the thirteen automatic landing flights were applied to the control surface exiting test, including four trials of elevator-exciting test for a longitudinal aerodynamic model identification and two trials each of aileron and rudder exciting test for a lateral-directional model identification.

Although a dynamic flight could be conducted in the automatic landing flight tests by utilizing the equilibrium glide phase, a quasi-steady flight could not be performed in the automatic landing flight which lasts only some 40 seconds and requires a precise landing because a quasi-steady flight needs a longer time period and the flight path will be shifted

from the reference trajectory due to large variation of the angle of attack and the side slip angle. So the equilibrium glide data obtained from the five flights in which control surface exciting tests were not performed were used to evaluate trimmed flight characteristics.

3.2 Aerodynamic Characteristics Estimated from Automatic Landing Flights

Tables 3.2-1 and 3.2-2 show the model structures used for aerodynamic model identification using the dynamic flight data obtained in the automatic landing flights and parameter values of an analytical model obtained by fitting these model structures to the flight test data (hereinafter referred to as the "AL identified model") with the parameters of a predicted model obtained based on the wind tunnel test results. The reason why the longitudinal model structures are expanded at α =8° is that the estimated model parameters should be evaluated at α =8° because the vehicle flies at around this value of the angle of attack during the equilibrium glide phase. During the maneuver, the angle of attack and the side slip angle vary between 4 and 11 degrees and ±2 degrees, respectively. These ranges are rather small because the α / β step input tests could not be performed in the automatic landing flight tests, as they were in the hanging flight tests. To compensate for this, the flight data during the path capture phase are also used for the identification, and the total variation range of the angle of attack is between 0 and 20 degrees. Following this, the longitudinal predicted model was extracted by fitting the model structure to the wind-tunnel model between the range of the angle of attack from 0 to 20 degrees. As the lateral-directional predicted model was obtained based on the wind-tunnel model at the angle of attack of 8 degrees, predicted parameter values shown on the Table

Table 3.2-1 Longitudinal Aerodynamic Model (Automatic Landing Flight)

Longitudinal Aerodynamic Model Structure, α_0 = 0.1396 rad (= 8 deg)

$$C_L = C_{L_0} + C_{L_\alpha}\cdot(\alpha-\alpha_0) + C_{L_{\delta e}}\cdot\delta e + C_{L_{\delta s}}\cdot\delta s$$
$$C_D = C_{D_0} + C_{D_{\alpha 2}}\cdot(\alpha-\alpha_0)^2 + C_{D_\alpha}\cdot(\alpha-\alpha_0) + C_{D_{\delta e}}\cdot\delta e + C_{D_{\delta s}}\cdot\delta s$$
$$C_m = C_{m_0} + C_{m_{\alpha 2}}\cdot(\alpha-\alpha_0)^2 + C_{m_\alpha}\cdot(\alpha-\alpha_0) + C_{m_q}\cdot\hat{q} + C_{m_{\delta e}}\cdot\delta e + C_{m_{\delta s}}\cdot\delta s$$

Longitudinal Aerodynamic Model Parameters

	C_{L_0}	$C_{L_{\alpha 2}}$	C_{L_α}	C_{L_q}	$C_{L_{\delta e}}$	$C_{L_{\delta s}}$
Prediction (Tolerance)	0.208 (0.022)	–	2.206 (0.401)	–	0.723 (0.180)	−0.074
Estimation (3σ)	0.175 (0.002)	–	2.202 (0.011)	–	0.415 (0.032)	−0.020 (0.004)

	C_{D_0}	$C_{D_{\alpha 2}}$	C_{D_α}	C_{D_q}	$C_{D_{\delta e}}$	$C_{D_{\delta s}}$
Prediction (Tolerance)	0.075 (0.007)	1.157	0.200	–	0.105	0.054
Estimation (3σ)	0.076 (0.000)	1.274 (0.012)	0.181 (0.004)	–	−0.019 (0.004)	0.051 (0.001)

	C_{m_0}	$C_{m_{\alpha 2}}$	C_{m_α}	C_{m_q}	$C_{m_{\delta e}}$	$C_{m_{\delta s}}$
Prediction (Tolerance)	0.008 (0.010)	−0.277	0.034 (0.121)	−0.794	−0.244 (0.060)	0.017
Estimation (3σ)	0.003 (0.000)	−0.179 (0.003)	0.019 (0.001)	−0.768 (0.028)	−0.224 (0.002)	0.011 (0.000)

Table 3.2-2 Lateral-Directional Aerodynamic Model (Automatic Landing Flight)

Lateral-Directional Aerodynamic Model Structure

$$C_Y = C_{Y_0} + C_{Y_\beta}\cdot\beta + C_{Y_{\delta a}}\cdot\delta a + C_{Y_{\delta r}}\cdot\delta r$$
$$C_l = C_{l_0} + C_{l_\beta}\cdot\beta + C_{l_p}\cdot\hat{p} + C_{l_r}\cdot\hat{r} + C_{l_{\delta a}}\cdot\delta a + C_{l_{\delta r}}\cdot\delta r$$
$$C_n = C_{n_0} + C_{n_\beta}\cdot\beta + C_{n_p}\cdot\hat{p} + C_{n_r}\cdot\hat{r} + C_{n_{\delta a}}\cdot\delta a + C_{n_{\delta r}}\cdot\delta r$$

Lateral-Directional Aerodynamic Model Parameters (α =8°)

	C_{Y_0}	C_{Y_β}	C_{Y_p}	C_{Y_r}	$C_{Y_{\delta a}}$	$C_{Y_{\delta r}}$
Prediction (Tolerance)	0.001 (0.006)	−0.654 (0.111)	–	–	−0.043 (0.010)	0.191 (0.063)
Estimation (3σ)	0.001 (0.000)	−0.883 (0.027)	–	–	−0.173 (0.020)	0.227 (0.010)

	C_{l_0}	C_{l_β}	C_{l_p}	C_{l_r}	$C_{l_{\delta a}}$	$C_{l_{\delta r}}$
Prediction (Tolerance)	−0.000 (0.004)	−0.181 (0.034)	−0.269	0.074	−0.142 (0.022)	0.064 (0.017)
Estimation (3σ)	0.000 (0.000)	−0.115 (0.004)	−0.190 (0.014)	0.074	−0.133 (0.003)	0.055 (0.001)

	C_{n_0}	C_{n_β}	C_{n_p}	C_{n_r}	$C_{n_{\delta a}}$	$C_{n_{\delta r}}$
Prediction (Tolerance)	−0.001 (0.001)	−0.048 (0.023)	0.121	−0.436	0.044 (0.014)	−0.108 (0.024)
Estimation (3σ)	−0.001 (0.000)	−0.020 (0.005)	0.121	−0.226 (0.050)	0.038 (0.003)	−0.106 (0.002)

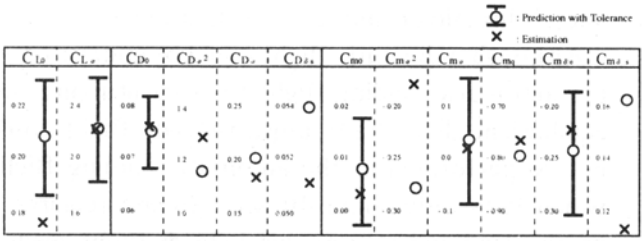

Fig. 3.2-1 Longitudinal Model Parameters (Automatic Landing Flight)

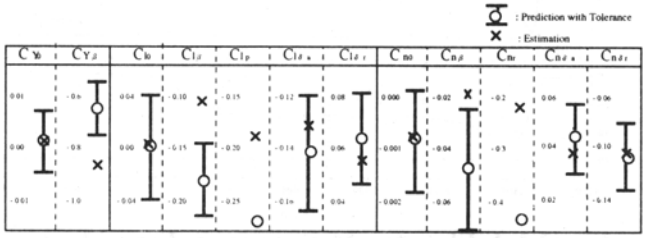

Fig. 3.2-2 Lateral-Directional Model Parameters (Automatic Landing Flight)

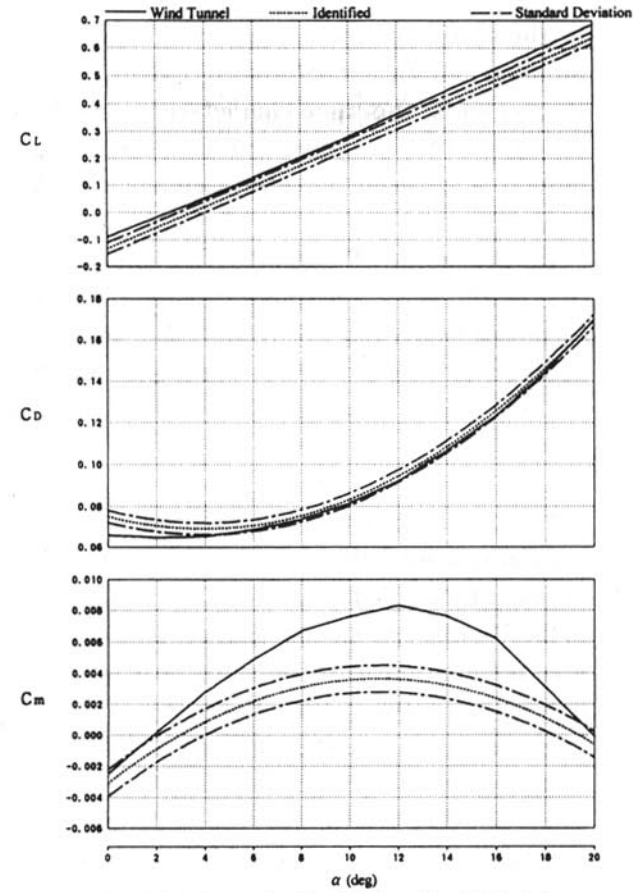

Fig. 3.2-3 Longitudinal Identified Model (Automatic Landing Flight)

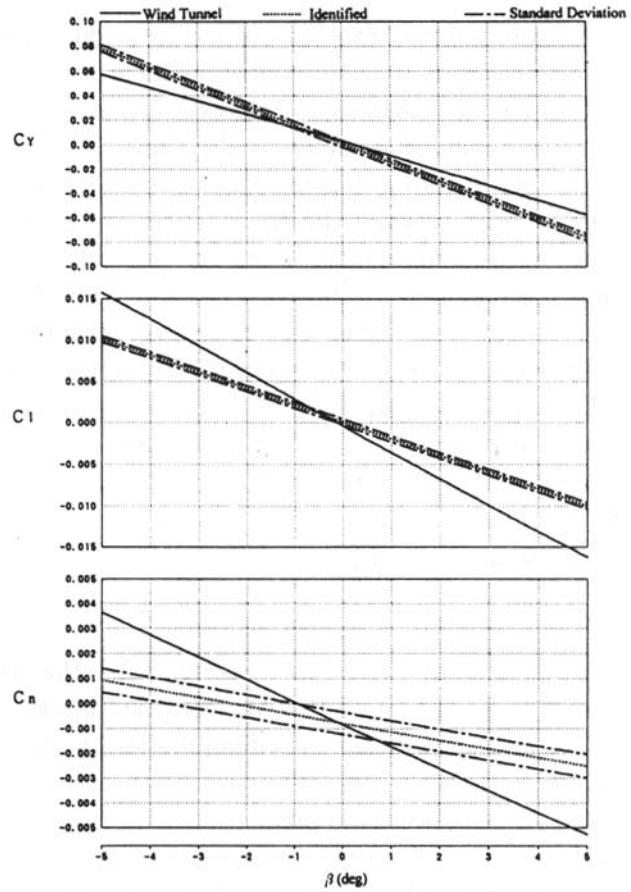

Fig. 3.2-4 Lateral-Directional Identified Model (Automatic Landing Flight)

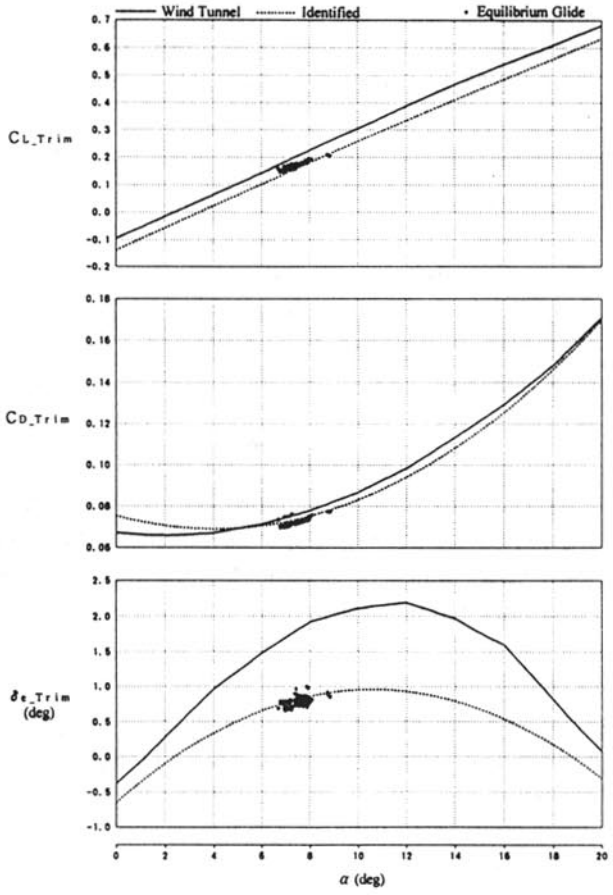

Fig. 3.2-5 Estiamted Longitudinal Trim Characteristics (Automatic Landing Flight)

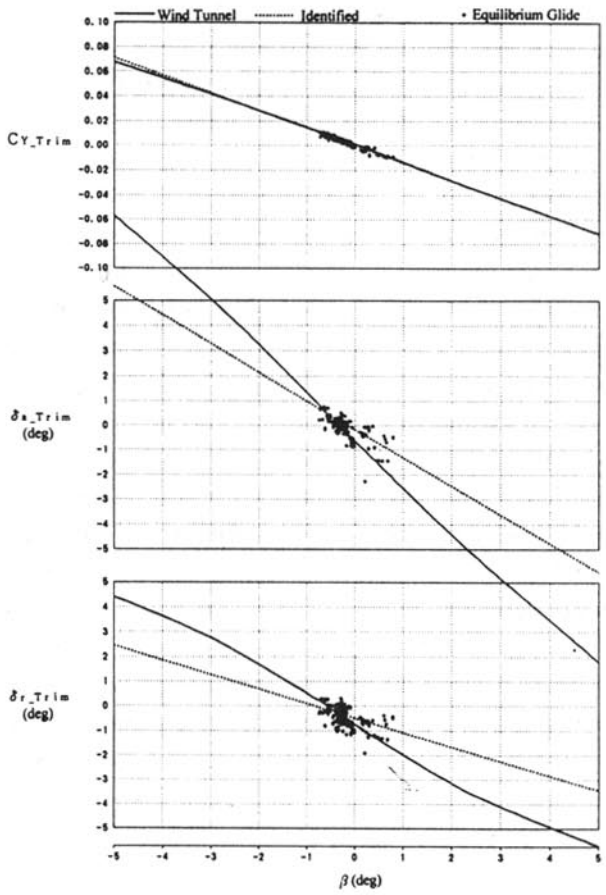

Fig. 3.2-6 Estiamted Lateral-Directional Trim Characteristics (Automatic Landing Flight)

3.2-2 are different from those shown in the Table 2.2-2 (based on the wind-tunnel model at the angle of attack of 0 degrees). Figures 3.2-1 and 3.2-2 show the major parameters in the Tables 3.2-1 and 3.2-2 graphically. Figures 3.2-3 and 3.2-4 show the relation between the AL identified model and the wind-tunnel model using α or β as an abscissa parameter. Figures 3.2-5 and 3.2-6 show the trimmed characteristics calculated using these two models and those extracted from the five flights in which the control surface exciting tests were not performed. The notation of these figures and tables are the same as those in section 2.2. The following are the results of a study of these figures and tables.

(1) Longitudinal Characteristics

Judging from Table 3.2-1 or Fig. 3.2-1 the lift curve slope (CL_α) of the AL identified model is closer to the predicted slope than the HF identified model. However, the difference of the constant term (CL_0) between the predicted and the estimated value is 150% of the tolerance and the difference of an elevator effect ($CL_{\delta e}$) is 170% of the tolerance. These differences are larger than those in the case of the hanging flights. In the parameters concerning the drag coefficient, there is no bias between the estimated and the predicted values, which was seen in the case of the hanging flight, and the differences of other parameters are smaller than those in the hanging flights. The speedbrake effect ($CD_{\delta s}$) of the identified model is 95% of the predicted value. In the parameters concerning the pitching moment coefficient, the differences between the identified and predicted parameters are the same or smaller than the hanging flights. The identified pitch damping (Cm_q) is 97% of the predicted value and the elevator effect ($Cm_{\delta e}$) is 91%, which are fairly near to the predicted value.

In Fig. 3.2-3, the bias of the lift coefficient seen is remarkable. The drag coefficient of the AL identified model is much closer to the wind-tunnel model than the HF identified model and a scattering of the input data for the identification indicated with dash-dot lines is also much smaller which means that the obtained data are better because the input data are free from measurement errors caused by the tension of the hanging wire. The pitching moment coefficient of the AL identified model shows almost the same characteristics as those of the HF identified model and there seems to be a difference between the identified and wind-tunnel models.

In the graph of trimmed characteristics (Fig. 3.2-5), the characteristics extracted from the AL identified model coincide with those extracted from equilibrium glide data of the five flights, and there is no discordance which is seen in the HF identified model.

(2) Lateral-Directional Characteristics

Judging from Table 3.2-2 or Fig. 3.2-2, there is no bias of the side force coefficient, which was seen in the HF identified model and seems to be caused by measurement error of the gimbal roll angle. The differences between the parameters of the AL identified model and the predicted model are similar to the HF identified model for parameters other than β derivatives, but the differences in β derivatives of all the three coefficients are outside the tolerances. This is because β step input tests could not be performed in the automatic landing flights and the variation of the side slip angle was only between $\pm$ 2 degrees which made identification of β derivatives difficult.

In Fig. 3.2-4, the differences of β derivatives of the three coefficients are remarkable. A scattering of input data shown with dash-dot lines are smaller than the hanging flight.

Although Fig. 3.2-6 is valuable for the evaluation of aerodynamic unsymmetricalness, to this extent there is no discrepancy between the AL Identified model, the wind-tunnel model and the equilibrium glide data.

4. Summary of Results

The following is a summary of the above mentioned results of comparison of the wind tunnel data, the hanging flight estimation and the automatic landing estimation for each coefficient.

(1) Lift Coefficient

All the results of the lift curve slope (CL_α) are almost the same and they seem to be reliable.

Constant terms of the wind-tunnel data and the hanging flight estimation are almost the same, but the term of the automatic landing estimation are about 0.03 smaller than the others. The difference is beyond the tolerance of the wind-tunnel data. Although judging simply, the results of the hanging flights, which are closer to the wind-tunnel data are more reliable than those of the automatic landing flights, measurement errors of the former maybe larger because the latter is free from measurement errors caused by the tension of the hanging wire. Further study is necessary to clarify these results. As the effects of the elevator and the speedbrake ($CL_{\delta e}$,$CL_{\delta s}$) are rather small, the results for these two parameters extracted from the flight test data are not reliable.

(2) Drag Coefficient

In the results obtained from the hanging flights there are biases which are different from each flight and seem to be caused by the measurement error of the gimbal pitch angle, and good results were not obtained. However, the results of the automatic landing flights almost coincide with the wind-tunnel data, and the results are reliable. Although the effect of the speedbrake ($CD_{\delta s}$) is estimated only from the automatic landing flights, it is very near to the wind-tunnel data.

(3) Pitching Moment Coefficient

The characteristics against the angle of attack obtained from the hanging flights and the automatic landing flights are similar to each other but they are different from those of the wind-tunnel model, although the differences are within the tolerances of the wind-tunnel data. This means that either the wind-tunnel data or the results estimated from the flight tests have errors. If the estimated results extracted from the flight tests do have errors, one possible error is estimation error of the C.G. position. The C.G. position of the vehicle was estimated experimentally using the vehicle with the final configuration[3]. In the case that the C.G. position used for the analysis is shifted to the more unstable side (backward) from the real position, this kind of difference will be derived through the analysis. So the difference of C.G. position equivalent to the difference of the pitching moment characteristics obtained from the present analysis is calculated and the result is found to be 30 mm. Judging from two facts, that the experiment for C.G. position estimation does not seem to have this large error and that the results extracted from the hanging wind tunnel tests[2] agree with the results of the flight tests and there does not seem to be the same large error of C.G. position in the hanging wind-tunnel test, it may be concluded that the wind-tunnel database for the pitching moment have some error due to, for example, the effect of a supporting device.

(4) Side Force Coefficient

In the hanging flight, there is bias error and an error of β derivative. The former seems to be caused by the measurement error of the gimbal roll angle and is not seen in the automatic landing flight, but the latter in the automatic landing flights is larger than in the hanging flight. The reason for this is that the variation of the side slip angle is too small during the maneuver in the automatic landing flights. Both of the rudder derivatives ($CY_{\delta r}$) estimated from the hanging flight and the automatic landing flight are within the tolerances. The aileron derivatives ($CY_{\delta a}$) are estimated to be three to four times larger than the wind-tunnel database, but the reliability seems low because the effect of the aileron does not have a large effect on the vehicle's dynamics.

(5) Rolling Moment Coefficient

All the estimated parameters except for the β derivative (Cl_{β}) extracted by the automatic landing flights are inside the tolerance. The difference of the β derivative may be due to too small variation of the β during the maneuver, as in with the side force coefficient. The roll damping (Cl_p) is estimated at 70% to 75% of the wind-tunnel database. The aileron derivative ($Cl_{\delta a}$) is 85% to 94%, and a rudder derivative ($Cl_{\delta r}$) is 83% to 86%.

(6) Yawing Moment Coefficient

There is a large difference between the β derivative (Cn_{β}) estimated by the automatic flight tests and the wind-tunnel database, as with the

rolling moment. The estimated values of a yaw damping (Cn_r) by the hanging flights and the automatic flights are 52% and 74% of the wind-tunnel database. The aileron derivative ($Cn_{\delta a}$) is estimated at 104% to 86%, and the rudder derivative ($Cn_{\delta r}$) is 86% to 96%.

Judging from these, among the characteristics which are estimated from the flight test data and seem to be reliable, there are obvious differences between the estimated characteristics and the ones predicted from the wind-tunnel database for the bias of the lift coefficient and the pitching moment characteristic against the angle of attack. For the former difference, further analysis is necessary. For the latter difference, the wind-tunnel database seems to have some error, because all of the data except for the wind-tunnel database show the similar characteristics, but the difference is within the tolerance. In the hanging flights, the estimated results for the drag coefficient and the side force coefficient were scattered due to the measurement errors of the gimbal pitch and roll angle caused by the effects of the umbilical cable. The characteristics except for the above are estimated well by the hanging flights, including the effects of control surfaces and the dynamic effects, and the method was shown to be useful. More accurate estimation will be possible if the effect of the umbilical cable can be reduced by using an inner battery, for example.

5. Conclusion

The estimated aerodynamic characteristics are similar to the wind-tunnel database except for the bias of the lift coefficient and beta derivatives of the lateral-directional aerodynamic coefficients. For the lift coefficient, it is not clear which is correct the estimated one or the database and further analysis is necessary. For the lateral-directional characteristics, the estimated beta derivatives seem to have error due to too small variation of the side slip angle during the maneuver. Although the difference of the pitching moment coefficient between the estimated characteristics and the wind-tunnel database is smaller than the uncertainties of the database, it is concluded the estimated characteristics show more accurate characteristics of the vehicle.

References

1) Nagayasu, M. et al.; On the Automatic Landing Flight Experiment (ALFLEX), Proceedings of the ALFLEX Symposium (1997)

2) Nagayasu, M. et al.; On the Interactive Computer Program IPIS for Aircraft Parameter Identification, Technical Report of National Aerospace Laboratory TR-1000 (1988) (In Japanese)

3) Yanagihara, M. et al.; Suspending Wind-Tunnel Test for ALFLEX Vehicle, Technical Report of National Aerospace Laboratory TR-1306 (1996) (In Japanese)

4) Tsukamoto, T. et al.; Estimation of ALFLEX C.G. position, Technical Memorandum of National Aerospace Laboratory (1997) (In Japanese)